Structural Basis of Motility in the Microtubular Axostyle: Implications for Cytoplasmic Microtubule Structure and Function

D. T. WOODRUM and R. W. LINCK
Department of Anatomy, Harvard Medical School, Boston, Massachusetts 02115

ABSTRACT The gross morphology of the protozoan microtubule axostyle of *Saccinobaculus ambloaxostylus* can now be described in macromolecular detail. The left-handed coil of the axostyle is seen to be dependent upon the asymmetry inherent in the constituent microtubules as expressed by the specific array of linkages between microtubules and by a possible tendency for microtubules to coil into left-handed helices. The laminated sheets of microtubules are not aligned parallel to the long axis of the organelle, but become increasingly tilted off-axis as one descends through the sheets of microtubules from the convex to the concave surface of the axostyle.

Fine-structural analysis of the axostyle indicates similarities of the linkages to dynein. The potential loci of the force-generating protein(s) are discussed as well as implications of the axostyle's structure on general microtubule function.

Certain species of protozoa found in the hindgut of the wood-feeding roach, *Cryptocercus punctulatus*, possess a motile organelle known as the axostyle. Compositionally simplistic, the axostyle consists of thousands of singlet microtubules interconnected by linkages to form rows spanning the width of the axostyle. This organelle has been described as a ribbon of microtubules oriented longitudinally, thus parallel to the edge of the axostyle (5, 16, 28, 30). The axostyle of *Saccinobaculus ambloaxostylus*, one species of these polymastigote hindgut protozoa, is composed of 30–60 sheets of microtubules (28). This species can propagate undulating bends along the length of its axostyle as well as produce a motion that is a repetitive coiling and then extending of the whole axostyle (9; and footnotes 1 and 2). Presumably the protozoan manipulates specific regulating parameters to select for one or the other type of motion. Undulating bends in the axostyle were thought to occur by sliding between adjacent rows of microtubules mediated by projections thought to be dynein-like (5, 25, 30). Cross-bridges with a 16-nm axial repeat that connect adjacent microtubules within a row have also been described (6, 16), but have been assigned no specific function.

This paper in particular will elucidate the complex structure of the axostyle of *S. ambloaxostylus* and present evidence that the constituent microtubules are not aligned parallel to the edge of the axostyle. Also, the fine structure of axostyle cross-bridges in general will be presented, which evokes discussion of the true locus of the dynein-like protein, the possible force-generating roles of the intrarow vs. interrow arms, and the relationship of microtubule structure and polarity in force generation.

[1] M. S. Mooseker, personal communication.
[2] D. T. Woodrum, unpublished observations.

MATERIALS AND METHODS

Woodroaches of the species *C. punctulatus* were collected at the Mountain Lake Biological Station of the University of Virginia, Mountain Lake, Virginia. In the laboratory, they were housed in covered plastic containers filled with partially rotted oak and other hardwoods.

Isolation of Protozoa and Axostyles

Gut contents taken from the hindgut of *C. punctulatus* were diluted with Trager's solution U (36) and then differentially centrifuged at low speed (600–1,000 rpm) in a clinical centrifuge, to select the axostyle-bearing species of protozoa (5). These protozoa were demembranated by addition of 0.5% Nonidet P-40, 0.1 M KCl, 20 mM Tris, pH 7.0, 2.5 mM $MgSO_4$, 0.5 mM EDTA, and 5 mM dithiothreitol (DTT). The isolated axostyles were washed in this wash solution minus the Nonidet two times. 2 mM ATP was added to the wash solution to yield axostyles predominantly in the coiled figuration.

Negative Stain

A drop containing isolated unfixed axostyles was placed on a carbon-film grid, washed with the wash solution, and stained with 1% uranyl acetate according to the procedure of Huxley (19).

THE JOURNAL OF CELL BIOLOGY · VOLUME 87 NOVEMBER 1980 404-414

Thin Section

Demembranated, isolated axostyles were fixed as a pellet in 1% glutaraldehyde, 1% tannic acid, 10 mM NaH_2PO_4, pH 7.0, at room temperature for 24 h. After a brief wash with 10 mM NaH_2PO_4, pH 6.0, the pellets were postfixed with 1% OsO_4, 10 mM NaH_2PO_4, pH 6.0, at 4°C for 40 min, dehydrated with a graded series of cold ethanols, and embedded in Epon. Thin sections were examined in a JEOL 100CX electron microscope operated at 80 kV.

Scanning Electron Microscopy

Nonidet-isolated axostyles were glutaraldehyde-fixed in suspension and then suctioned onto a nucleopore filter via a sidearm filter apparatus. The filter carrying the axostyles was then washed, postfixed with 1% OsO_4 for 30 min, washed with distilled water four times, then immersed in a freshly made, filtered, saturated solution of thiocarbohydrazide in distilled water for 15 min. After four more distilled-water rinses, the filter was again immersed in 1% OsO_4 in water for 15 min, then dehydrated in cold ethanols and critical point dried from ethanol with liquid CO_2 as the transition fluid. In some cases, a thin coating of gold-palladium was evaporated onto the dried sample. The axostyles were observed in a JEOL 100CX electron microscope with the high-resolution scanning attachment.

Rapid Freezing and Freeze-Fracture

Intact, actively beating protozoa were prepared as a concentrated slurry and quick-frozen by slamming against an ultrapure block of copper cooled to 4°K. The design and operation of the apparatus for freezing were similar to that described by Heuser et al. (18). The rapidly frozen samples were stored in liquid nitrogen until transfer to a Balzers' BAF 301 freeze-fracturing device (Balzers Corp., Nashua, N. H.). The freeze-fracturing of the samples and the formation of platinum-carbon replicas were performed according to standard techniques.

Polarization Microscopy

A Zeiss photomicroscope equipped with polarizer, analyzer, and a λ/30 Brace-Köhler rotary compensator was used to observe isolated axostyles. A xenon lamp was used as the source.

RESULTS

Orientation and Arrangement of Microtubules in the Axostyle

Axostyles isolated in the presence of ATP appear in the light microscope as coiled ribbons. Polarization microscopy reveals that the orientation of maximum extinction is oblique to the edge of the axostyle (Fig. 1). Because microtubules are strongly form birefringent (34) and account for >75% of the mass of the axostyle (as estimated from EM cross sections), the birefringence data suggested to us that the orientation of the microtubules was oblique to the edge of the axostyle (39). Polarization microscopy of live material yields important information as to the microtubule orientation, but in the event that all microtubules are not parallel, it provides an averaged value of their orientation. We therefore have studied the problem further, using high-resolution scanning electron microscopy.

The isolated axostyle of *S. ambloaxostylus* is seen by scanning electron microscopy (Fig. 2 *a*) to be a left-handed helix of 1.5–2 turns, composed of concentric sheets of microtubules. The microtubules on the exterior surface run in an almost perfectly longitudinal manner along the helical circumference (Fig. 2 *b*). The outermost sheet is narrower than the immediate sheets underneath, giving a step-layered edge (Fig. 2 *b*), which in cross section presents a step-wise row ending (Fig. 4 *a* and *b*). Close examination reveals ends of microtubules at both edges of each sheet. The ends of microtubules on the upper edge (Fig. 2 *c*) all point anteriorly, and the ends of those on the lower edge all point posteriorly (data not shown). The frequency of ends per sheet increases as one proceeds from the outermost to the innermost observable sheet, suggesting that the orientation of microtubules becomes more and more oblique in each successively inner sheet and that the microtubules become progressively shorter. The microtubules of the outermost sheet are oriented almost parallel to the edge of the axostyle and are therefore the longest microtubules, whereas each inner sheet of the axostyle can be described as a parallelogram of approximately constant-length microtubules with the ends of the microtubules forming the edge of the axostyle. That this is indeed the case is demonstrated by Fig. 2 *d*, which is a view of the inner surface of the helix. The wood-grain or topographical map appearance of the inner surface of the axostyle is quite striking in contradistinction to its outer surface. However, the same systematic change in the orientation of microtubules is true for this inner surface if one thinks of it as a continuation of the properties and processes expressed by the outer sheets. Each successive inner sheet is composed of progressively shorter, more numerous and slightly more tilted microtubules than the adjacent outer sheet.

The angle of microtubules in one sheet relative to those in an adjacent sheet is shallow and is ~1°, an average of 17° between the tubules 15 sheets apart (see Fig. 2 *d*). It is possible that the adjacent sheet-to-sheet tilt is not constant throughout the thickness of the axostyle, however, and the tilt may be graded instead. The arrangement of microtubules in the coiled axostyle as seen by scanning electron microscopy therefore confirms and explains their apparent off-axis orientation as first observed by polarization microscopy.

A simplified diagram of the arrangement of sheets and the

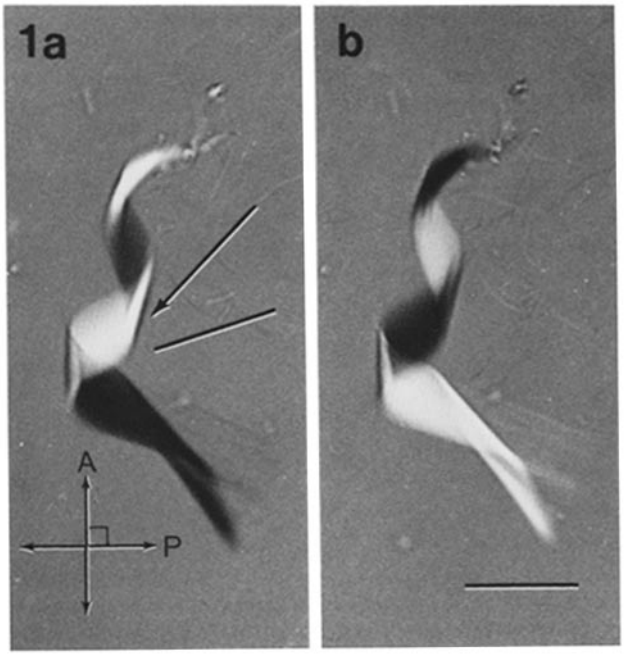

FIGURE 1 Polarization micrograph of an isolated axostyle presented in bright and dark contrast. Fig. 1 *a* gives the appearance that the axostyle is coiled in a right-handed helix. This is an optical illusion caused by the bright and dark contrast. The viewer subjectively selects the bright-contrast portion to be proximal as if illuminated and the dark-contrast portion to be distal as if in shadow. A reversal of the contrast in Fig. 1 *b* reverses this effect, yielding the image of a left-handed helix. The axostyle naturally presents as a left-handed helix as shown in Fig. 2 *a*. The fine bar is aligned with the lower edge of the axostyle and the arrow indicates the orientation of maximum extinction, ~26° from the lower edge. The orientations of the analyzer (*A*) and polarizer (*P*) are indicated at the lower left. Bar, 8 μm.

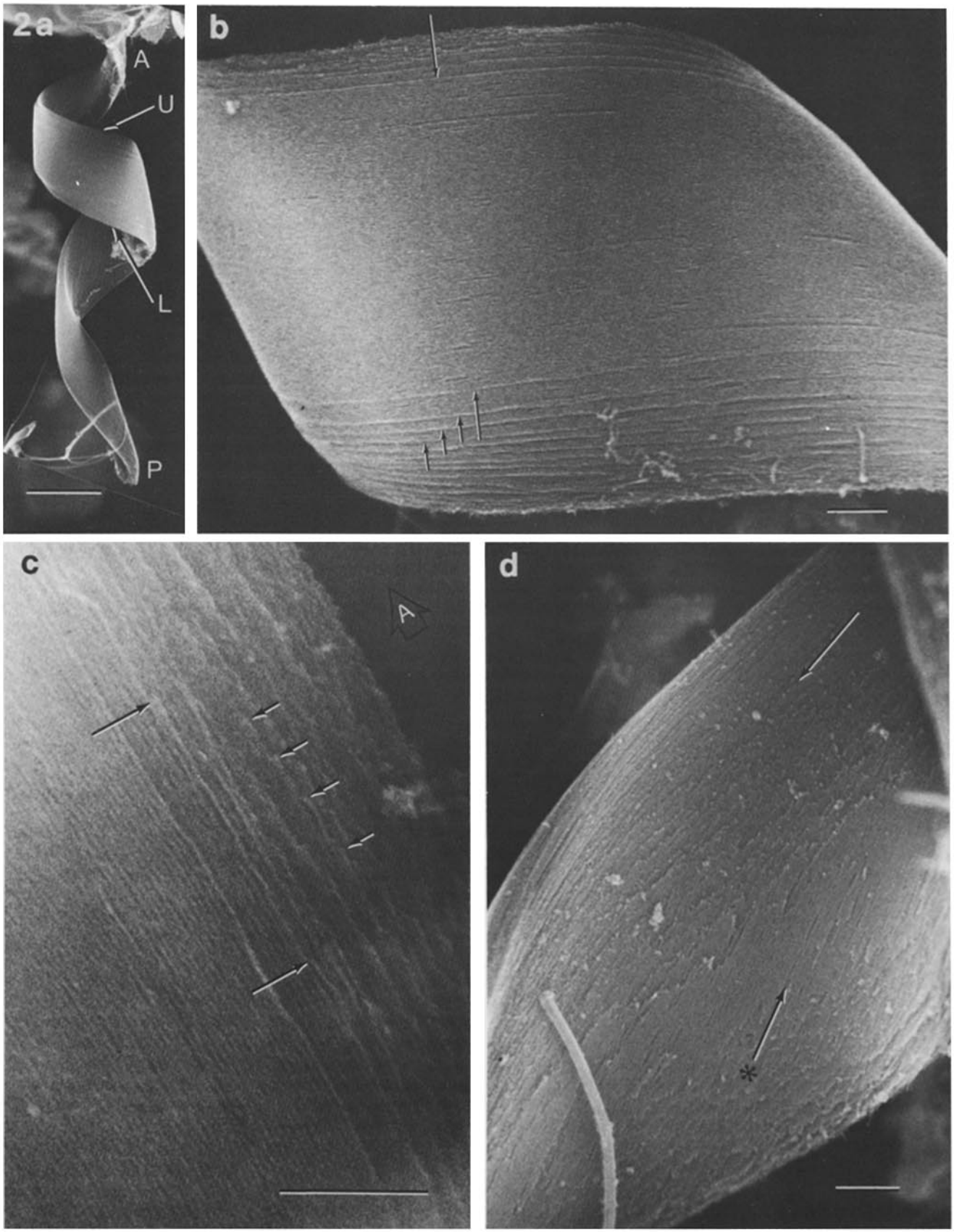

orientation of microtubules in a coiled axostyle of *S. ambloaxostylus* is presented in Fig. 3. At this point the reader is advised to study this diagram.

In "cross section", the coiled axostyle displays a characteristic crescent-shaped array of microtubules. Fig. 4*a* is an axostyle of *S. ambloaxostylus* in cross section, the approximate plane of which is indicated in Fig. 3; a similar image would be produced by sectioning the axostyles of Fig. 2*b* or *d* across their widths. To some extent, this crescent shape is a result of the natural curvature of the sheets, here viewed as rows of cross-sectional microtubules, across the width of the axostyle. Overlying the inherent curvature of the sheets, however, is the effect of shaping the axostyle into a helix. Thus there are two components contributing to the crescent shape that are difficult to separate when viewing a cross-sectional image.

The step-layered edge of the axostyle seen earlier in scanning EM (Fig. 2*b*) is readily evident in cross section in Fig. 4*a* and *b* as a step-wise row ending on the outer or convex surface of the axostyle. That the two edges in this crescent are not similarly tapered is a result of the angle of the section through the axostyle and the extent of skewing or slipping of the inner sheets toward the upper or lower edge of the axostyle. This skewing may be discerned in Fig. 2*d* where the inner sheets are slightly displaced more towards the lower edge of the axostyle as defined in Fig. 2*a*.

The increasing tilt of the successive sheets of microtubules through the thickness of the axostyle is also apparent in Fig. 4*b*, which is a higher magnification of the left side of the axostyle in Fig. 4*a*. One readily observes that the microtubules in the outer rows (on the convex surface) appear in exact cross section, whereas those of the inner rows become progressively more oval and blurred, indicating they are tilted out of the plane of section. In addition, a less pronounced blurring of the microtubule cross-sectional appearance also occurs within a single row moving from left to right. This effect arises because: (*a*) the individual microtubules follow left-handed helical paths, (*b*) adjacent microtubules are staggered anteriorly-posteriorly within a sheet, and (*c*) the whole array of sheets of microtubules is formed into the helix of the coiled axostyle.

Fine Structure of Intermicrotubule Linkages

There are at least two sets of linkages holding the microtubules in a semicrystalline array (Fig. 4*c*). One set consists of intrarow cross-bridges connecting the microtubules into rows (sheets). The second set consists of interrow projections emanating from the microtubules in one sheet and projecting toward the microtubules in the next innermost sheet. These projections have been described as the locus for the dynein found associated with the axostyle (5, 30). Neither of these structures has been previously studied by negative-stain electron microscopy.

Fig. 5*a* and *b* is a negative-stain image of a sheet of microtubules. The prominent cross-bridges between adjacent microtubules measure ~7-nm thick by 18–22 nm long and are arranged with an axial periodicity of 16 nm along the tubules. These structures are oriented at various tilt angles of up to 30°–40° relative to a line normal to the microtubule axes. Areas can also be seen where the cross-bridges are almost perpendicular to the microtubules, i.e., 0° tilt. In negative stain a bright dot appears at the end of but slightly out of register with the cross-bridges and may correspond to a foreshortened view of the interrow projection (see below).

In an effort to view the structure of the cross-bridges and projections in the living state and to understand their mechanical roles in motility, we have applied the techniques of rapid freeze, deep etch, and rotary shadowing to the axostyles of unfixed, actively motile cells. Because only a small portion of an axostyle is presented in any fracture face, precise identification of the protozoan species is not possible. In Fig. 5*c* and *d*, the 16-nm axial periodicity of the cross-bridges between microtubules is prominent, as is the relatively constant angle of cross-bridge tilt (20°). In Fig. 5*e* and *f*, which is a different area from the same axostyle in Fig. 5*c* and *d*, the cross-bridges are seen to be almost perpendicular to the microtubules. It is of interest to note that although the cross-bridge angles vary, they are essentially identical between any given set of two microtubules over a distance of 0.5 μm. We do not at present know whether there is a preferred direction of tilt (polarity) of the cross-bridges.

Fig. 5*c–f* clearly shows the substructure of the cross-bridges and the substructure in the wall of the microtubule. In such rotary-shadowed preparations, the cross-bridges measure 8 nm thick by 18–22 nm long and appear to be composed of a linear arrangement of 7-nm globular subunits.

In the rapid-frozen, rotary-shadowed specimens (Figs. 5*c–f*), a torus-shaped structure appears at one end of the cross-bridge. The torus-shaped component in these figures, measur-

FIGURE 2 Scanning electron micrographs (SEM) of isolated axostyles. (*a*) Low magnification view of isolated axostyle, *A*, anterior end; *P*, posterior end; *U*, upper edge; *L*, lower edge. (*b*) Exterior surface of an isolated axostyle. The concentric sheets are of varying widths: the outermost sheet, indicated by the two opposed arrows, is narrower than the several sheets underneath (single arrows). This characteristic change in the width of the sheets on the exterior surface gives rise to a step-layered edge indicated here by the set of four arrows and seen in cross section in Fig. 4 *b*. Microtubules within the outer sheet run almost longitudinally within the sheet and are the longest microtubules. (*c*) High-resolution detail from the upper edge. This axostyle was processed for SEM via the thiocarbohydrazide method. There was no subsequent metal shadowing. The longer arrows indicate two ends of adjacent microtubules in the second sheet. Progressively more ends of microtubules can be seen in each successively deeper sheet. The four shorter arrows indicate the ends of four adjacent microtubules in the sixth sheet. The microtubule ends can be seen to best advantage by tilting the page and sighting along the axes of the microtubules. Note that the ends all point anteriorly (denoted by *A* within black arrowhead) in this upper edge. (*d*) A view of the inner surface of the helical axostyle seen by SEM. The innermost sheet is composed of the shortest and most tilted microtubules, and can best be approximated by a parallelogram with the ends of the microtubules forming the long edges of the parallelogram. Each successive sheet towards the exterior surface of the axostyle can also be described as a parallelogram except that each sheet is composed of progressively longer microtubules. The arrows are aligned with the microtubules of two different sheets. From the innermost sheet, indicated by the arrow with an asterisk, to another sheet 15 sheets toward the exterior, indicated by the plain arrow, the change in microtubule tilt is 17°. The microtubules of the innermost sheet are also tilted 38° relative to the lower edge of the axostyle. A flagellum overlies the axostyle at the lower left. Bars: *a*, 8 μm; *b–d*, 1 μm.

ing ~10 nm in diameter, may be a terminal subunit of the cross-bridge. Thus, this image of the cross-bridges and associated structures is produced by observing the sheet of microtubules from the convex surface (see Fig. 4). On the other hand, the three-dimensional relief of the replica in Fig. 5*g* clearly presents the projections viewed end-on and also seen as toruses sitting to one side of the microtubule. The intrarow cross-bridges in Fig. 5*g* are deeper in the fracture replica than the projections in agreement with the relative positioning of these two different structures as seen in the cross-sectioned axostyles (Fig. 4*c*). This view of the cross-bridges and the less regular projections is produced by observing the sheet of microtubules from the concave surface. Occasionally two projections can be seen sitting side by side and slightly staggered on the same microtubule (bold arrows, Fig. 5*g*). This positioning of two adjacent projections on the same side of a microtubule is occasionally seen in cross-sectioned axostyles as indicated by the doublet arrows in Fig. 4*c*. Bloodgood and Miller (6) observed dual projections in one image of a cross-fractured axostyle, but were uncertain of there being two projections. Fig. 5*g* clearly shows that slightly staggered dual projections do, in fact, exist, although the frequency of these, as well as the frequency of individual projections, is low.

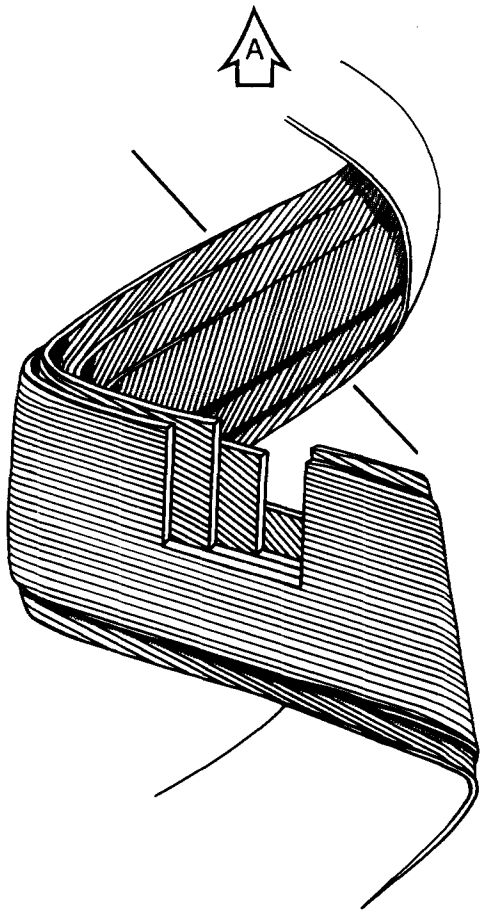

FIGURE 3 A simplified diagram of the arrangement of sheets and the orientation of microtubules in a coiled axostyle of *S. ambloaxostylus*. Only four sheets are depicted from an axostyle 40 sheets thick. Each sheet diagrammed has a different width and is 10 sheets apart from the next diagrammed sheet. The orientation of microtubules within each sheet is indicated by parallel lines. Given an ~1° tilt per sheet of microtubules as seen in Fig. 2 *d*, each representative 10th sheet in this diagram is therefore tilted 10° more obliquely than the previous representative sheet as one descends through the thickness of the axostyle from the outer to the inner surface. The microtubules of the outermost sheet appear to be approximately parallel to the edge of the axostyle and are the longest microtubules, whereas the microtubules of the innermost sheet are tilted 40° from the lower edge of the axostyle and are the shortest. The width of each sheet is specified by the length, number, and tilt of the constituent microtubules. Note that the successive inner rows are composed of progressively more, albeit shorter, microtubules. Each sheet, in addition, is represented by a coiled-up parallelogram with the ends of the microtubules on the upper edge all pointing anteriorly and the ends on the lower edge pointing posteriorly in agreement with the SEM observations (Fig. 2). The diagonal line marked on opposite sides of the axostyle width and perpendicular to the outer sheet of microtubules indicates the approximate plane of section of Fig. 4 *a* and *b*. The reader should note that in such a cross-sectional view of the axostyle the microtubules of the outer sheet would be in perfect cross section, whereas those of successive inner sheets would become more and more oblique to the direction of view; the expected results are experimentally obtained (Fig. 4 *a* and *b*).

DISCUSSION

Orientation and Arrangement of Microtubules in the Axostyle of S. ambloaxostylus

The observed pattern of microtubules lends insight into the form and function of the axostyle. The structure of the axostyle can most simply be described as a helical coil of concentric, laminated sheets of microtubules. The scanning electron microscope images (Fig. 2) best describe this structure, yet a few important points should be noted. Each sheet can be described as a parallelogram. The outermost sheet of tubules forms a coiled-up parallelogram in which the tubules are oriented almost parallel to the edge of the axostyle ribbon. Each successive inner sheet is composed of microtubules that are of an approximately constant length within each sheet but are somewhat shorter and more obliquely arranged relative to the previous sheet. Each successive sheet of microtubules thus also forms a coiled-up parallelogram in which ultimately (on the inner aspect of the axostyle) the long edge of the parallelogram is composed of thousands of ends of microtubules (Figs. 2*d* and 3).

McIntosh et al. (28) noted that in *S. ambloaxostylus* the adjacent sheets (rows) in cross section were tilted laterally by 0.5° from one sheet to the next. This tilt was attributed to the difficulty of packing many adjacent sheets into one helix with a pitch of 100 μm and a radius varying from about 5 to 7 μm, i.e., to the passive lateral slip between concentric sheets upon coiling. Thus, just as when one twists a stack of computer cards into a helix, there is some slewing or slipping between the cards to accomodate the coil. The geometrical constraints of a number of sheets forming a helix probably does account for some of the tilt of adjacent sheets; however, that is a less than accurate account of the whole pattern of obliquely oriented microtubules. The tilted arrangement of the microtubules within successive sheets is a fundamental feature of the axostyle structure, leading to shorter and more obliquely oriented microtubules (Fig. 2*d*) and is not merely a result of passive slip between sheets. Furthermore, the tilted arrangement of the microtubular sheets may be architecturally important in the supramolecular assembly of the axostyle by providing a mechanism for the formation of the appropriate bond angles and distance relationships between the curved sheets of microtubules.

Some change in the degree of tilt of successive sheets across

the thickness of the axostyle may accompany the passing of a bend along the length of the axostyle, in which case the tilt may be an important transitory event during a specific phase of motion. As can be deduced from Fig. 2*d*, however, the microtubules of most sheets could not be aligned perfectly longitudinally with respect to the long axis of the axostyle.

The arrangement of individual microtubules in each sheet and the overall form of the axostyle exhibit a curious enantiomorphic asymmetry to which several factors contribute. First, the individual microtubules with their associated components are cylindrically asymmetric. This asymmetry is apparent because in cross section (Fig. 4*c*) a single "unit cell" is composed of a 13-protofilament microtubule that possesses at precise points about its circumference at least four different axial rows of binding sites: one for the proximal end of the cross-bridge, one for the proximal end of the projection, and two for the attachment of the distal ends of these same structures, which originate from the two interacting intrarow and interrow microtubules. Thus, just as the enantiomorphic asymmetry of the 9+2 flagellar axoneme is defined by the direction of skewing of the doublet tubules and the orientation of the dynein arms (1, 15), so then is the enantiomorphic form of the axostyle defined by the direction and orientation of the cross-bridges and projections, i.e., whether the distal end of each cross-bridge points clockwise or counter-clockwise along the circular arcs (rows) when a cross section of the axostyle is viewed from its anterior end. We have not yet defined the correct enantiomorph in the axostyle; nevertheless, current work indicates that the underlying lattice of subunits in the wall of all microtubules may be helically asymmetric.[3, 4]

A second feature of the axostyle's enantiomorphic asymmetry is that the axostyle is in the form of a left-handed helix (Fig. 2*a*) (9, 28, 30), and thus the individual microtubules must also follow a left-handed helical path. This left-handed helical shape must certainly be related to the tendency of flagellar microtubules to twist into left-handed helices (29, 41), and this property may in turn be related to the above-mentioned lattice asymmetry of microtubules.

Finally, the arrangement of the microtubules in each sheet exhibits an enantiomorphic asymmetry that is fundamental to the axostyle. If one views the inner sheet of microtubules from inside the axostyle helix (as in Fig. 2*d*), the microtubules are seen to be aligned to produce for each sheet a parallelogram of unique form. From the perspective just outlined, one observes that the anteriormost microtubule in each sheet has for its adjacent microtubule in that sheet one that is located spatially more posterior and to the left. Presumably, this precise spatial relationship of adjacent microtubules within a sheet is mediated by the positioning of linkage proteins and their interactions with the microtubules. In conclusion then, the natural form of the axostyle is seen to result from the inherent cylindrical asymmetry of the microtubules, their tendency to coil in a left-handed manner, and specific properties that govern their interactions (e.g., the various microtubule linkage proteins). Perhaps if the underlying asymmetry of the individual microtubules were reversed, a completely mirrored, right-handed axostyle would result.

[3] Linck, R. W., and G. L. Langevin. Reassembly of flagellar $B_{\alpha\beta}$-tubulin into singlet microtubules: consequences for cytoplasmic microtubule structure. Manuscript submitted for publication.

[4] Linck, R. W., G. E. Olson, and G. L. Langevin. Arrangement of tubulin subunits and microtubule-associated proteins in the central pair microtubule apparatus of squid (*Loligo pealeî*) sperm flagella. Manuscript submitted for publication.

Existence and Locus of the Force-transducing Components

We use the term force-generating components to refer to proteins directly involved in the hydrolysis of ATP, whereas the term force-transducing components includes force-generating proteins but also proteins that act subsequently to couple the application of force to movement. There are two prominent sets of microtubule-associated components in the axostyle that are considered to be the most likely candidates for force generation (Fig. 4*c*). Each axostyle microtubule possesses a single or double row (depending on species) of structures that form cross-bridges with adjacent microtubules within a row: we refer to these as intrarow cross-bridges. Each microtubule also possesses a single or double row of structures that project toward the microtubules of the adjacent inner row; we refer to these as interrow projections. We use the terms cross-bridges and projections without intending to imply any mechanical function to these two components.

The intrarow cross-bridges have only been observed in the bridged state and always appear to be uniformly thick, i.e., 8 nm thick by 18–22 nm long (16, 28, 30, and this report). On the other hand, the interrow projections do not always appear uniform in cross-section; i.e., they do not always appear long enough (usually 2 nm) to span the 20- to 26-nm gap between rows of tubules. It is not clear in cases where the gap is spanned whether this appearance is an artifact or results from an extended or better preserved projection or from another intermicrotubule filamentous linkage superimposed over the projection.

Mooseker and Tilney (30) and Bloodgood (5) reported that isolated axostyles contain ATPase activity with properties similar to those of sea urchin sperm flagellar dynein (11, 13) and that isolated axostyles contain a polypeptide that comigrates with one of the heavy chains of sea urchin sperm flagellar dynein (12, 20–22). The structural locus of the purported axostyle dynein was presumed to be the interrow projections (5, 25, 30), although no evidence supports or refutes this presumption. Our Fig. 5*g* shows a striking morphological similarity between the 10-nm torus-shaped projection and the individual subunits of *Tetrahymena* ciliary dynein arms (9.3 nm in diameter) isolated and negatively stained (38). Yet, the platinum replicas of rapid-frozen live axostyles shown in Fig. 5 also reveal two important similarities between the intrarow cross-bridges and the dynein arms of cilia and flagella. First, the cross-bridge is composed of three to four linearly arranged globular subunits, each ~7–8 nm in diameter; such an appearance is morphologically similar to the subunit appearance of negatively stained intact *Tetrahymena* ciliary dynein arm subunits measuring 7.8 nm center-to-center, (38). Second, one sees the cross-bridges at various angles relative to a line normal to the microtubule axis (0°–40°). We have observed the tilt of the cross-bridges in both rapid-frozen live protozoa and axostyles isolated in the presence of ATP. In agreement with Bloodgood and Miller (6) and McIntosh (26), cross-bridges between two interacting microtubules all appear to have the same angle of tilt along a given length of microtubule (along 0.5 μm or ~30 cross-bridge repeats; Fig. 5*a*, *c*, and *e*), but the angle of these groups of cross-bridges varies from region to region within the same speciment (Fig. 5*c* vs. *e*). Using thin-section and negative-stain EM, other investigators have observed that, in the absence of ATP, ciliary and flagellar dynein arms form cross-bridges between adjacent doublet microtubules (14, 35, 37, 40). The angles of the dynein arm cross-bridges are tilted toward the

ciliary/flagellar base by 30°, which is remarkably similar to the maximum angle we observe for cross-bridges in rapid-frozen (Fig. 5 *c*) or negative-stained (Fig. 5 *a*) axostyles. In the case of axostyles, however, we do not know the absolute polarity of the cross-bridge tilt. Although a change in angle of the axostyle cross-bridges with respect to the microtubule axis is not proof of a force-generating mechanism, such angle changes are consistent with the hypothesis that sliding can occur between microtubules within a sheet. Interestingly, there is as yet no evidence to suggest that these axostyle cross-bridges ever detach from the bridged microtubules.

The three-dimensional wave motion of a single beating axostyle can assume several different forms, for example, rapid, reversible coiling vs. undulating waves vs. a rotating polygon (9, 16, 28, 30; and footnote 2). We suggest that interactions between microtubules via both the cross-bridges and the projections must be involved in the particular mode of beat. Because the loci of the dynein-like protein remain uncertain, models proposing sliding between sheets also remain equivocal. Thus, the suggestion can be put forth that sliding between microtubules within a sheet is a component of force-transduction for in vivo movement of the axostyle. But it remains to be determined whether the actual force is generated by the cross-bridges, by the projections, or by both.

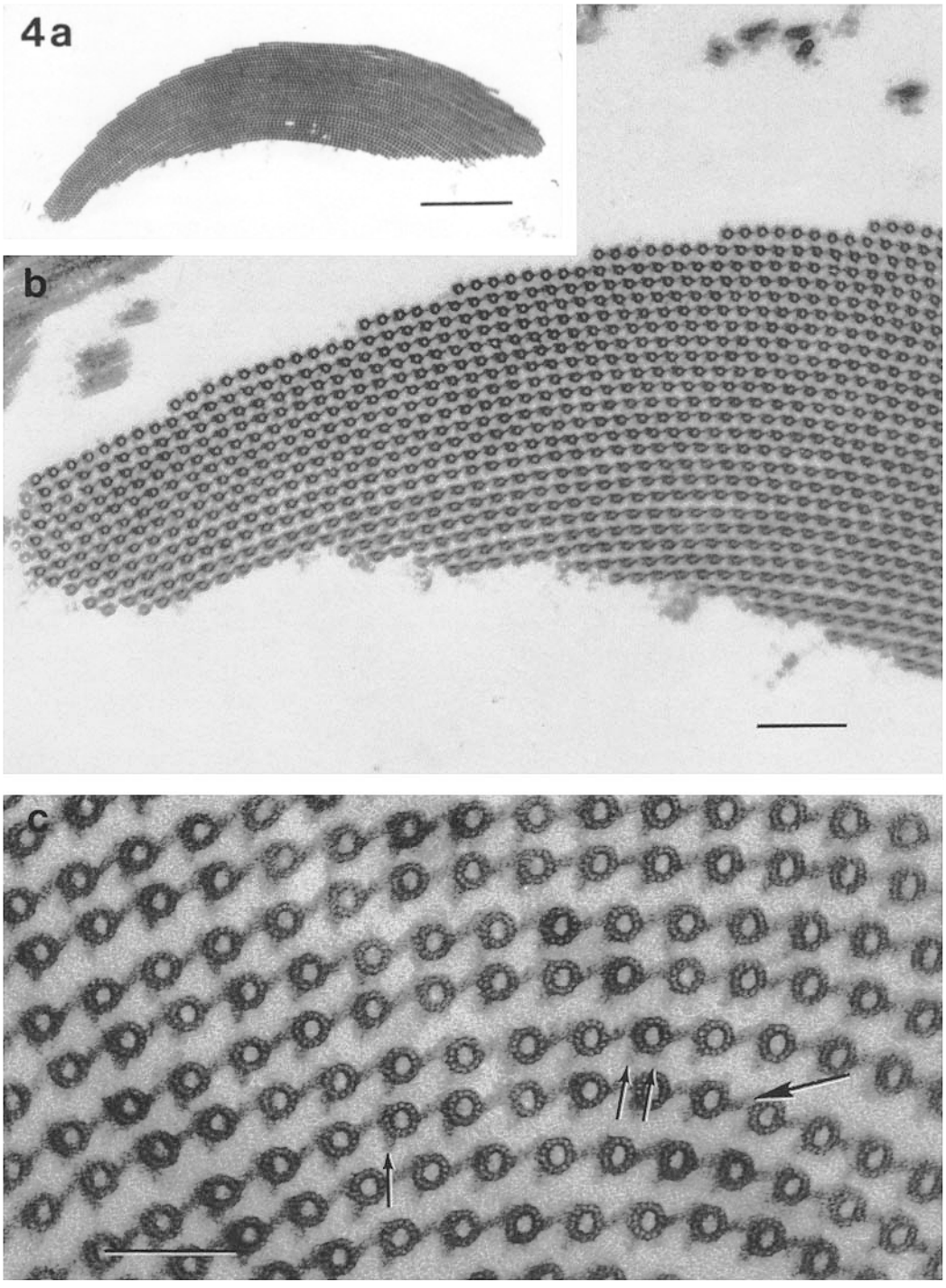

Implications for General Microtubule Function

Regardless of whether the intrarow cross-bridges, the interrow projections, or both are the sites of force generation, a few comments are necessary concerning the possible relationship of these structures to dynein. Axostyle cross-bridges repeat along the microtubule with a 16-nm axial periodicity, whereas ciliary and flagellar dynein arms of most species repeat with a 24-nm axial spacing (for review, see reference 23). The axostyle microtubules also possess ~16-nm axially spaced binding sites for the projections; however, the frequency of bound projections is randomly interrupted by unoccupied sites, as elegantly put forth by McIntosh (26). Such differences in the spacing of these axostyle components from that of dynein along the microtubule do not alone rule out that these structures are dynein analogues, as the information for spatial determination may reside in a dynein "tail" or a separate linear spacer molecule possessing both dynein and microtubule binding sites. Alternatively, the tubulin lattice of the axostyle microtubules may be altered to yield a 16-nm repeat of the dynein attachment site. Nevertheless, axostyle dynein may have unique properties, and one must consider these in relation to reports of dynein-like proteins isolated from sea urchin eggs and sea urchin egg mitotic apparatuses (32, 33) and from brain tissue (8, 10, 31).

Finally, perhaps most importantly, a consideration of the axostyle and ciliary and flagellar axonemes allows us to make several predictions that are of fundamental importance to microtubule structure and to dynein-mediated mechanisms of microtubule motility in general. First, in the typical 9+2 axoneme of cilia and flagella, the dynein arm of one doublet microtubule (n) attaches at its base to the A-tubule, evidently composed of an A-lattice of tubulin dimers (3), and interacts with a B-lattice on the B-tubule of the adjacent (n+1) doublet microtubule. The axostyle, on the other hand, is composed exclusively of singlet microtubules. Thus, making the highly probable assumption that the axostyle microtubules are structurally and chemically identical to each other (except for length), the cross-bridges and/or projections must take their origins from and interact with the same type of microtubule. This situation predicts that the axostyle singlet microtubules possess components of both A and B lattices. Our recent findings in fact indicate that cytoplasmic singlet microtubules in general are asymmetric, possessing lattice discontinuities in the form of seams between pairs of protofilaments.[3, 4]

Our last point concerns the relevance of microtubule polarity to force generation of microtubule organelles. Again assuming that axostyle microtubules are structurally identical (except for length), an antiparallel arrangement of either adjacent microtubules within a sheet or of alternate sheets of microtubules is sterically impossible; i.e., all axostyle microtubules are aligned with the same structural polarity. Our prediction then is that in microtubular organelles force generation is developed between microtubules with the same polar orientation. Our conclusions are deduced from the following observations: (*a*) the distal (+) ends of both A- and B-subfibers of flagellar doublet microtubules nucleate and elongate singlet microtubules at a rate greater than that of the proximal (−) ends, and the direction of the assembly designates the underlying structural polarity (2, 4, 7); and (*b*) reassembled brain microtubules decorated with flagellar dynein associate sterospecifically in a unipolar manner (17). Thus, we conclude that in hypothetical mechanisms suggesting sliding interactions between microtubules, any requirement for antiparallel microtubules would seem unnecessary. Furthermore, models of mitosis (24, 27) involving sliding of antiparallel microtubules should be reevaluated.

The authors thank Dr. Elio Raviola for his help with the rapid-freezing studies and Dr. D. Lansing Taylor for assistance with preliminary polarization microscopy.

This work was supported by an Albert J. Ryan Fellowship to D. T. Woodrum and by a National Institute of General Medical Sciences grant (GM21527) to R. W. Linck.

Received for publication 21 April 1980, and in revised form 14 July 1980.

FIGURE 4 (*a*) A low-magnification micrograph of an axostyle of *S. ambloaxostylus* cut in cross sections, i.e., across the width of the axostyle. The plane of section is perpendicular to the tenth outermost row of microtubules measured from the convex surface of the crescent-shaped axostyle; this plane of section is indicated approximately by the diagonal line to either side of the axostyle diagrammed in Fig. 3. The crescent shape of the axostyle shown here arises both from the fact that the microtubules are linked together into circular arcs (rows) and from the fact that this is a section through a helical ribbon. The concave side of the crescent faces the interior of the helix as seen in Fig. 2 *a*. In cross section the edges of the axostyle appear tapered as predicted by the SEM (Fig. 2) and the model (Fig. 3). Note that the left- and right-hand edges are not symmetrical, possibly indicating a slipping or skewing of inner rows of microtubules in a lateral direction toward the upper or lower edge. (*b*) A higher magnification image of the left side of *a*. The step-wise row ending is evident on the outer or convex surface of the crescent-shaped axostyle. A row is defined by the linking together of microtubules by cross-bridges (see *c*) into circular arcs. Note that in cross section the concave surface appears artificially to be composed of rows of progressively fewer microtubules; however, as evidenced by the SEM view of the concave surface in Fig. 2*d*, the rows are actually composed of more (albeit shorter) microtubules than the rows on the convex surface. This apparent dearth of microtubules in the inner surface rows results from the angle at which these obliquely arranged rows of microtubules are sectioned. The progressive tilt of adjacent rows from the outer to the inner surface of the axostyle can be seen as the orientation of the sectioned microtubules changes from perfect circular cross sections (outer rows) to more oblique and thus blurred ovals (inner rows). In addition, a blurring of the microtubule cross-sectional appearance also occurs to a lesser extent within a single row moving from left to right in this figure. This effect arises because: (*1*) the individual microtubules follow left-handed helical paths, (*2*) adjacent microtubules are staggered anteriorly-posteriorly within a sheet, and (*3*) the whole array of sheets of microtubules is formed into the helix of the coiled axostyle. (*c*) Cross-section of a tannic acid–fixed axostyle different from the one in *a* and *b*. The two types of linkages are indicated by arrows. The large arrow indicates a cross-bridge between adjacent microtubules within a sheet. The cross-bridges link adjacent microtubules into rows (sheets) as seen in cross section. The small arrows indicate projections extending from the microtubules of one sheet to the microtubules of the next innermost sheet. Occasionally seen extending the distance between sheets in this micrograph, the projections in this axostyle number one per microtubule or possibly two (double arrow); such single and doublet sets of projections are seen in longitudinal view in Fig. 5 *a* and *g*. Bars: *a*, 1 μm; *b*, 200 nm; *c*, 100 nm.

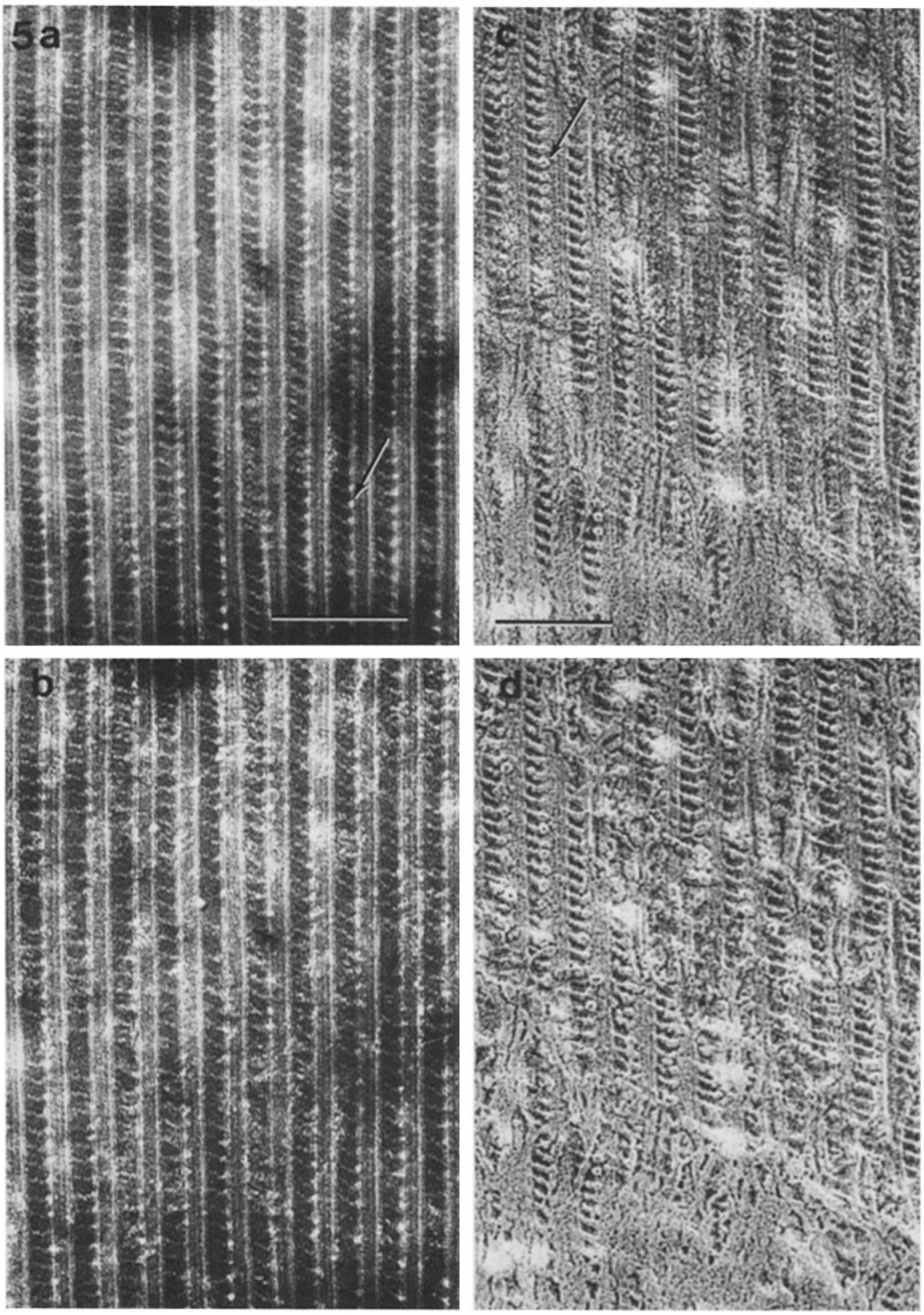

FIGURE 5 (*a* and *b*) Negative-stain image of a sheet of axostyle microtubules; *a* is a one-step, linear photographic translation of *b* equal to the repeat distance between cross-bridges. The cross-bridges are the prominent 16-nm axially repeating linkages between adjacent microtubules (unmarked). Note the display of angles made by the cross-bridges normal to the tubule axes. Cross-bridge angles vary from 0° to 40° but are essentially identical between any given set of two tubules. The arrow indicates a globular structure attached to the microtubule. Such globular structures most likely correspond to the projections seen in Figs. 4 and 5 *g*, here appearing superimposed over the left side of the tubule and slightly out of register with the cross-bridges. (*c* and *d*) Rapid-freeze, deep-etch, rotary-shadowed image of an unfixed axostyle; *c* is a one-step, linear photographic translation of *d* equal to the repeat distance between cross-bridges. The view is of the convex surface of a sheet of microtubules. The tilted 16-nm axially repeating cross-bridges are readily evident between adjacent microtubules. The structure of the cross-bridges suggests that they are composed of three to four linearly arranged 7- to 8-nm subunits. The arrow indicates one of a number of torus-shaped structures, 10 nm in diameter, which may be a terminal subunit of the cross-bridge. Note also the substructure in the wall of the

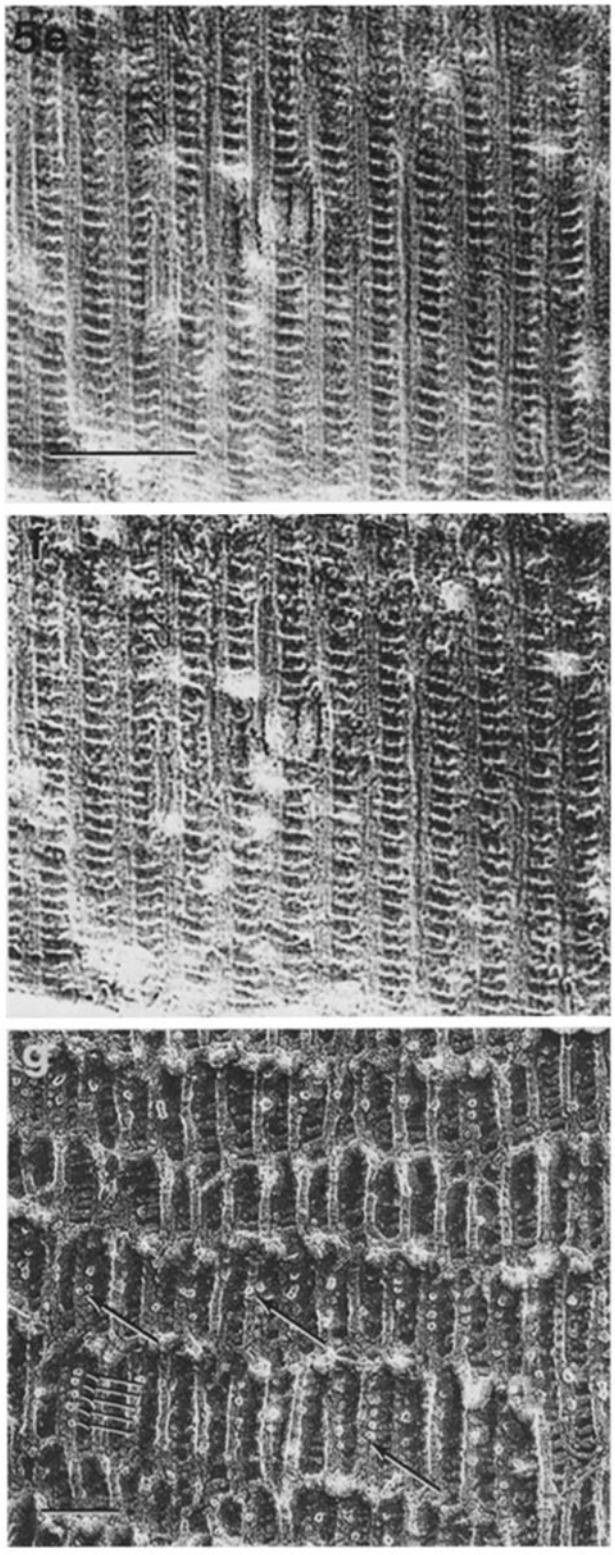

microtubule. (*e* and *f*) A different area from the same rapid-freeze, deep-etch, rotary-shadowed axostyle in *c* and *d*; *e* is a one-step, linear translation of *f* equal to the repeat distance between cross-bridges. The 16-nm axially repeating cross-bridges in this image are nearly perpendicular to the microtubule axes; again the cross-bridges appear to be composed of three to four linearly arranged 7- to 8-nm subunits. (*g*) A rapid-freeze, deep-etch, rotary-shadowed image of an unfixed axostyle different from the one in *c* and *e*. The five small arrows indicate a row of projections seen end-on and positioned to one side of the underlying microtubule; each projection appears to be torus-shaped in this profile and measures 10 nm in diameter in rotary-shadowed replicas. The three bolder arrows indicate examples of dual projections similar to those in Fig. 4 *c*. Intrarow cross-bridges (unmarked) can be seen between microtubules, particularly in the upper right-hand corner of the micrograph. The wave-front appearance running horizontally across the replica demarcates where the fracture plane has jumped from one sheet of microtubules to the next adjacent sheet. Bars, 140 nm.

REFERENCES

1. Afzelius, B. 1959. Electron microscopy of the sperm tail. results obtained with a new fixative. *J. Biophys. Biochem. Cytol.* 5:269–278.
2. Allen, C., and G. G. Borisy. 1974. Structural polarity and directional growth of microtubules of *Chlamydomonas* flagella. *J. Mol. Biol.* 90:381–402.
3. Amos, L. A., and A. Klug. 1974. Arrangement of subunits in flagellar microtubules. *J. Cell Sci.* 14:523–549.
4. Binder, L. I., and J. L. Rosenbaum. 1978. The in vitro assembly of flagellar outer doublet tubulin. *J. Cell Biol.* 79:500–515.
5. Bloodgood, R. A. 1975. Biochemical analysis of axostyle motility. *Cytobios.* 14:101–120.
6. Bloodgood, R. A., and K. R. Miller. 1974. Freeze-fracture of microtubules and bridges in motile axostyles. *J. Cell Biol.* 62:660–671.
7. Borisy, G. 1978. Polarity of microtubules of the mitotic spindle. *J. Mol. Biol.* 124:565–570.
8. Burns, R. G., and T. D. Pollard. 1974. A dynein-like protein from brain. *FEBS (Fed. Eur. Biochem. Soc.) Lett.* 40:274–280.
9. Cleveland, L. R., S. R. Hall, E. P. Saunders, and J. Collier. 1934. The wood-feeding roach, *Cryptocercus*, its protozoa, and the symbiosis between protozoa and roach. *Mem. Am. Acad. Arts Sci.* 14:185–342.
10. Gaskin, E., S. B. Kramer, C. R. Cantor, R. Adelstein, and M. L. Shelanski. 1974. A dynein-like protein associated with neurotubules. *FEBS (Fed. Eur. Biochem. Soc.) Lett.* 40:281–286.
11. Gibbons, I. R., and E. Fronk. 1972. Some properties of bound and soluble dynein from sea urchin sperm flagella. *J. Cell Biol.* 54:365–381.
12. Gibbons, I. R., E. Fronk, B. H. Gibbons, and K. Ogawa. 1976. Multiple forms of dynein in flagellar axonemes of sea urchin sperm. *Cold Spring Harbor Conf. Cell Proliferation.* 3(Book C):915–932.
13. Gibbons, B. H., and I. R. Gibbons. 1972. Flagellar movement and adenosine triphosphatase activity in sea urchin sperm extracted with Triton X-100. *J. Cell Biol.* 54:75–97.
14. Gibbons, B. H., and I. R. Gibbons. 1974. Properties of flagellar "rigor waves" formed by abrupt removal of adenosine triphosphate from actively swimming sea urchin sperm. *J. Cell Biol.* 63:970–985.
15. Gibbons, I. R., and A. V. Grimstone. 1960. On flagellar structure in certain flagellates. *J. Biophys. Biochem. Cytol.* 7:697–716.
16. Grimstone, A. V., and L. R. Cleveland. 1965. The fine structure and function of the contractile axostyles of certain flagellates. *J. Cell Biol.* 24:287–400.
17. Haimo, L. T., B. R. Telzer, and J. L. Rosenbaum. 1979. Dynein binds to and crossbridges cytoplasmic microtubules. *Proc. Natl. Acad. Sci. U. S. A.* 76:5759–5763.
18. Heuser, J. E., T. S. Reese, M. J. Dennis, Y. Jan, L. Jan, and L. Evans. 1979. Synaptic vesicle exocytosis captured by quick-freezing and correlated with quantal transmitter release. *J. Cell Biol.* 81:275–300.
19. Huxley, H. E. 1963. Electron microscope studies on the structure of natural and synthetic protein filaments from striated muscle. *J. Mol. Biol.* 7:281–308.
20. Kincaid, H. L., B. H. Gibbons, and I. R. Gibbons. 1973. The salt-extractable fraction of dynein from sea urchin sperm flagella: an analysis by gel electrophoresis and by adenosine triphosphate activity. *J. Supramol. Struct.* 1:461–470.
21. Linck, R. W. 1970. A biochemical comparison of ciliary and flagellar axonemes from the bay scallop, *Aequipecten irradians. Biol. Bull. (Woods Hole).* 139:429.
22. Linck, R. W. 1973. Chemical and structural differences between cilia and flagella from the lamellibranch mollusc, *Aequipecten irradians. J. Cell Sci.* 12:951–981.
23. Linck, R. W. 1979. Advances in the ultrastructural analysis of the sperm flagellar axoneme. *In* The Spermatozoon: Maturation Motility, Surface Properties and Comparative Aspects. D. W. Fawcett and J. M. Bedford, editors. Urban and Schwarzenberg, Baltimore, Md. 99–115
24. Margolis, R. L., L. Wilson, and B. I. Kiefer. 1978. Mitotic mechanism based on intrinsic microtubule behavior. *Nature (Lond.)* 272:450–452.
25. McIntosh, J. R. 1973. The axostyle of *Saccinobaculus* II. Motion of the microtubule bundle and a structural comparison of straight and bent axostyles. *J. Cell Biol.* 56:324–339.
26. McIntosh, J. R. 1974. Bridges between microtubules. *J. Cell Biol.* 61:166–187.
27. McIntosh, J. R., P. K. Hepler, and D. C. VanWie. 1969. Model for mitosis. *Nature (Lond.).* 224:659–663.
28. McIntosh, J. R., E. S. Ogata, and S. C. Landis. 1973. The axostyle of *Saccinobaculus* I. Structure of the organism and its microtubule bundle. *J. Cell Biol.* 56:304–323.
29. Miki-Noumura, T., and R. Kamiya. 1979. Conformational change in the outer doublet microtubules from sea urchin sperm flagella. *J. Cell Biol.* 81:355–360.
30. Mooseker, M. S., and L. G. Tilney. 1973. Isolation and reactivation of the axostyle. Evidence for a dynein-like ATPase in the axostyle. *J. Cell Biol.* 56:13–26.
31. Murphy, D. B., and R. R. Hiebsch. 1979. Purification of microtubule protein from beef brain and comparison of the assembly requirements for neuronal microtubules isolated from beef and hog. *Anal. Biochem.* 96:225–235.
32. Pratt, M. M. 1980. The identification of a dynein ATPase in unfertilized sea urchin eggs. *Dev. Biol.* 74:364–378.
33. Pratt, M. M., T. Otter, and E. D. Salmon. 1980. Dynein-like Mg^{2+}-ATPase in mitotic spindles isolated from sea urchin eggs. *J. Cell Biol.* 86:738–745.
34. Sato, H., G. W. Ellis, and S. Inoué. 1975. Microtubular origin of mitotic spindle form birefringence. Demonstration of the applicability of Wiener's equation. *J. Cell Biol.* 67: 501–517.
35. Takahashi, M., and Y. Tonomura. 1978. Binding of 30S dynein with the B-tubule of the outer doublet of axonemes from *Tetrahymena pyriformis* and adenosine triphosphate induced dissociation of the complex. *J. Biochem.* 84:1339–1355.
36. Trager, W. 1934. The cultivation of a cellulose-digesting flagellate, *Trichomonas termopsidis*, and of certain other termite protozoa. *Biol. Bull. (Woods Hole).* 66:182–190.
37. Warner, F. D., and D. R. Mitchell. 1978. Structural conformation of ciliary dynein arms and the generation of sliding forces in *Tetrahymena* cilia. *J. Cell Biol.* 76:261–277.
38. Warner, F. D., D. R. Mitchell, and C. R. Perkins. 1977. Structural conformation of the ciliary ATPase dynein. *J. Mol. Biol.* 114:367–384.
39. Woodrum, D. T., and R. W. Linck. 1979. The structural basis of axostyle motility. *J. Cell. Biol.* 83(2, Pt. 2):179*a* (Abstr.).
40. Zanetti, N. C., D. R. Mitchell, and F. D. Warner. 1979. Effects of divalent cations on dynein cross-bridging and ciliary microtubule sliding. *J. Cell Biol.* 80:573–588.
41. Zobel, C. R. 1973. Effect of solution composition and proteolysis on the conformation of axonemal components. *J. Cell Biol.* 59:573–594.